Pigeons steer like helicopters and generate down- and upstroke lift during low speed turns

Ivo G. Ros[a,1], Lori C. Bassman[b], Marc A. Badger[b], Alyssa N. Pierson[b], and Andrew A. Biewener[a]

[a]Department of Organismic and Evolutionary Biology, Harvard University, Concord Field Station, 100 Old Causeway Road, Bedford, MA 01730; and [b]Department of Engineering, Harvey Mudd College, 301 Platt Boulevard, Claremont, CA 91711

Edited* by Mimi A. R. Koehl, University of California, Berkeley, CA, and approved October 24, 2011 (received for review May 12, 2011)

Turning is crucial for animals, particularly during predator–prey interactions and to avoid obstacles. For flying animals, turning consists of changes in (*i*) flight trajectory, or path of travel, and (*ii*) body orientation, or 3D angular position. Changes in flight trajectory can only be achieved by modulating aerodynamic forces relative to gravity. How birds coordinate aerodynamic force production relative to changes in body orientation during turns is key to understanding the control strategies used in avian maneuvering flight. We hypothesized that pigeons produce aerodynamic forces in a uniform direction relative to their bodies, requiring changes in body orientation to redirect those forces to turn. Using detailed 3D kinematics and body mass distributions, we examined net aerodynamic forces and body orientations in slowly flying pigeons (*Columba livia*) executing level 90° turns. The net aerodynamic force averaged over the downstroke was maintained in a fixed direction relative to the body throughout the turn, even though the body orientation of the birds varied substantially. Early in the turn, changes in body orientation primarily redirected the downstroke aerodynamic force, affecting the bird's flight trajectory. Subsequently, the pigeon mainly reacquired the body orientation used in forward flight without affecting its flight trajectory. Surprisingly, the pigeon's upstroke generated aerodynamic forces that were approximately 50% of those generated during the downstroke, nearly matching the relative upstroke forces produced by hummingbirds. Thus, pigeons achieve low speed turns much like helicopters, by using whole-body rotations to alter the direction of aerodynamic force production to change their flight trajectory.

biomechanics | tip reversal | aerodynamics | flapping flight | locomotion

Maneuverability is critical to the movement of animals in their natural environment. Turning represents a basic maneuver that is particularly relevant to predator–prey interactions and obstacle avoidance. To begin to understand the mechanisms by which birds achieve and control aerial turns, we examine the role of body rotations in relation to aerodynamic force production to alter the flight trajectory, or path of travel, during turns. More specifically, we ask whether body rotations serve to redirect aerodynamic forces during low speed 90° level turns in pigeons.

The three-dimensional (3D) nature of flight requires analyses of aerodynamic force production in relation to body motions not only in a global reference frame but also in a local, body reference frame (Fig. 1). The global frame allows for application of Newton's laws of motion, which for a flying bird means that the resultant of aerodynamic and gravitational forces can be estimated from accelerations of the whole-body center of mass (CM). However, the bird's torso moves relative to the CM, primarily due to the time-varying wing configurations during the wingbeat cycle. Therefore, localization of the CM cannot rely solely on the torso but requires detailed assessment of the motions of the head and wings as well. The body frame corrects for the displacements and rotations of the torso, allowing for analyses of head and wing motions and forces relative to the body, which subsequently can be related to underlying musculoskeletal and sensory-motor function. The combination of global and local frames therefore can reveal how aerodynamic force production is coordinated with a bird's 3D body orientation, or body angular position, during aerial turns.

There are two major reasons for animals to change their body orientations during turns: (*i*) to reacquire their preferred body orientation for forward movement and (*ii*) to alter the direction of propulsive force needed to change their movement trajectory. Bilaterally symmetric animals have body plans that are best suited for forward locomotion with a particular 3D body orientation (1). Consequently, this preferred body orientation must be reacquired during a turn to move along the new movement trajectory. Additionally, body rotations must also occur to redirect the animal's propulsive turning forces, if these forces are directionally constrained within the animal's body frame. Redirecting resultant forces in the global frame due to changes in body orientation is referred to as force vectoring (Fig. 1). In fact, flying insects have been argued to turn primarily by force vectoring, meaning that the majority of the redirection of aerodynamic forces is based on changes in body orientation and not on changes in the direction of aerodynamic forces relative to the insect's body (2).

Even though quantifying the time-varying aerodynamic forces produced during flapping flight is challenging, estimates of aerodynamic force production during flight maneuvers have been made in insects (3–7). Turning calliphorid, muscid, and drosophilid flies support the use of force vectoring as a means to redirect aerodynamic force as the aerodynamic forces produced by their wings operate within a limited range relative to their bodies. Most of the redirection of aerodynamic force within the body frame occurs within the animal's midsagittal plane, varying over a range of merely 20°, although fruit flies also generate moderate lateral forces with respect to their bodies. Notable exceptions are hover flies (Syrphidae), which seem to achieve a wider variation in aerodynamic force orientation relative to their bodies (8, 9), though these findings have been questioned (7).

Vertebrate fliers appear to also have a limited ability to redirect aerodynamic force relative to their bodies. Horseshoe bats, fruit bats, pigeons, and rose-breasted cockatoos roll during aerial turns (10–13), indicating that they likely rely on force vectoring to turn. Fruit bats rotate their bodies in the direction of the turn in addition to rolling, increasing their centripetal acceleration (13). Finally, pigeons appear to redirect aerodynamic forces to accelerate after flight takeoff and brake prior to landing by pitching movements of their bodies (14).

Here, we ask whether pigeons redirect aerodynamic forces (in the global frame) by redirecting aerodynamic forces relative to their bodies (Fig. 1*A*) or by rotating the body itself (Fig. 1*B*). Given the constrained musculoskeletal and stereotypical kinematic features of the avian wingstroke (15–18), we hypothesize that pigeons generate aerodynamic forces in a uniform direction relative to their bodies (i.e., in the body frame), necessitating the

Author contributions: I.G.R. and A.A.B. designed research; I.G.R. and A.A.B. performed research; I.G.R., L.C.B., M.A.B., and A.N.P. analyzed data; and I.G.R. and A.A.B. wrote the paper.

The authors declare no conflict of interest.

*This Direct Submission article had a prearranged editor.

[1]To whom correspondence should be addressed. E-mail: Ivo.Ros@gmail.com.

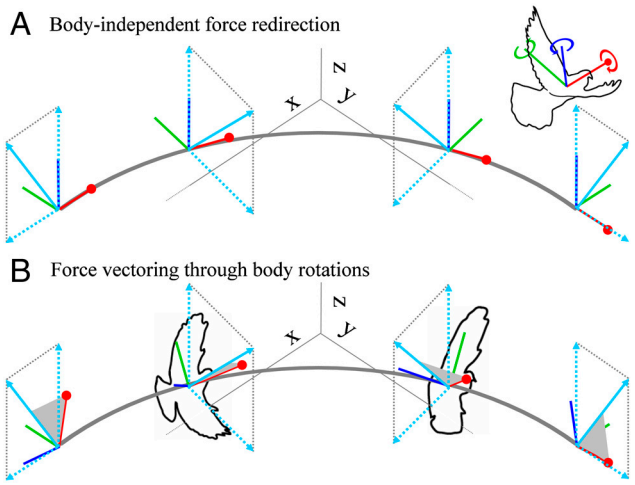

Fig. 1. Schematic representation of the experimental hypotheses. The global frame (thin gray lines) with z (vertical) defined in line with gravity and x and y defined along the two perpendicular horizontal axes of the flight corridor (Fig. 2). (*Upper Right Inset*) The bird's body frame with antero-posterior (along the spine), medio-lateral, and dorso-ventral axes in red, green, and blue, respectively. Rotations about these anatomical axes are defined as roll, pitch, and yaw (red, green, and blue circular arrows). (*A* and *B*) Hypothetical aerodynamic forces (solid light blue vectors) in the global frame during a level, 90° aerial turn to the right. Horizontal and vertical global projections (dashed blue vectors) of the aerodynamic forces early, during, and upon completion of the turn provide braking, centripetal, and accelerating forces, respectively, as well as vertical forces. (*A*) H_0: Birds produce aerodynamic forces in variable directions in the body frame, requiring only realignment of the antero-posterior body axis with the flight trajectory. (*B*) Force-vectoring hypothesis: Birds produce aerodynamic forces in a uniform direction in the body frame, requiring body rotations to redirect aerodynamic forces in the global frame to change flight trajectory (gray curved line). Note that the gray triangles shown between the antero-posterior body axis and resultant aerodynamic force vector are of identical dimensions in each of the four represented positions of the turn, emphasizing the anatomically fixed direction of aerodynamic force.

use of force vectoring to turn (Fig. 1*B*). To test this hypothesis, we used high-speed videography to obtain 3D positions of body markers of pigeons performing low speed, 90° level turns within a netted, 10m long, square-corner corridor (Fig. 2). Detailed analysis of the pigeons' whole-body mass distributions enabled their non-body-fixed CM to be accurately tracked, from which time-varying, whole-body, or net, aerodynamic forces were assessed (Figs. 2–5). To interpret the functional significance of changes in body orientation made throughout the turn, body rotations of the pigeons were quantified relative to the redirection of aerodynamic force averaged over successive downstrokes. Specifically, for each downstroke in the turn the component of the body rotation that redirected the average aerodynamic force was mathematically separated from the component of the 3D body rotation that had no effect on the direction of the average downstroke force. This approach allowed any 3D body rotation to be decomposed into two complementary body rotation fractions, one that redirected and one that rotated about the downstroke average aerodynamic force (Fig. 6).

Results

Three pigeons with a mean body mass of 319 ± 33 g (all results are expressed as mean $\pm$ SD) negotiated the 90° level turn at a CM speed of 3.3 ± 0.2 ms^{-1}, with mean flight trajectory slopes relative to the global horizontal plane of $2.5 \pm 0.2°$ and a wingbeat frequency of 8.3 ± 0.3 Hz. Combined wing mass distal to the shoulder comprised $12.5 \pm 1.4\%$ of total body mass.

Aerodynamic forces are reaction forces resulting from the interactions of the animal's body, wings, and tail with the surrounding air. In midair, an animal's flight trajectory can only be

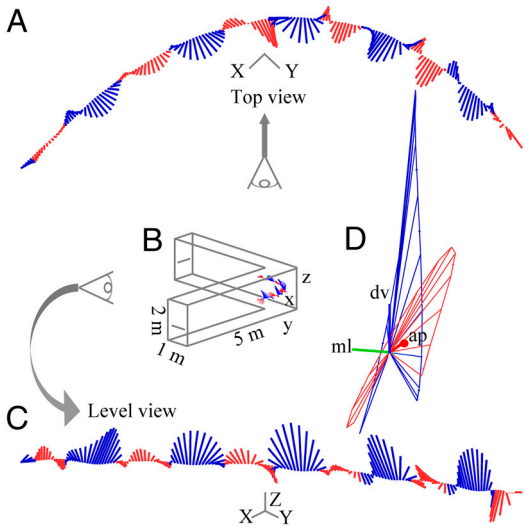

Fig. 2. Instantaneous net aerodynamic forces (**F**) visualized on corresponding center of mass (CM) positions throughout a representative right 90° turn. Downstroke forces in blue and upstroke forces in red, plotted at 4-ms intervals. (*A–C*) **F** in the global frame with axes *x*, *y*, and *z*. (*A*) Top view. (*B*) Schematic of the flight corridor with viewpoints for *A* and *C*. (*C*) Level view. (*D*) Caudo-lateral view of **F** for a single wingbeat in the body frame with antero-posterior (ap, red), medio-lateral (ml, green), and dorso-ventral (dv, blue) axes. Arrows connecting vector tips indicate temporal sequence. (*A*,*C*, and *D*) Axes lengths represent one body weight of force.

changed by gravity or the aerodynamic forces produced by the animal. Because the external force on an object equals the product of its mass and acceleration, the instantaneous aerodynamic force acting on the pigeon's center of mass (CM) can be estimated after factoring out gravity (see *Methods* for details). However, the time-varying configurations of the bird's wings and head relative to its torso cause the whole-body, or net, CM to vary in position with respect to the torso through time. This non-body-fixed CM therefore requires estimates based on detailed 3D kinematics and body mass distributions (Fig. 3). The mass-distribution model then provides estimates of instantaneous net aerodynamic forces (**F**) throughout the turns. The aerodynamic origin of these forces and any force components that cancel out internally, however, cannot be identified by this method.

Pigeons Turn with an Aerodynamically Active Upstroke. Throughout the 90° turn the pigeons produced aerodynamic forces during the upstroke as well as the downstroke (Fig. 2, 4). In the global frame,

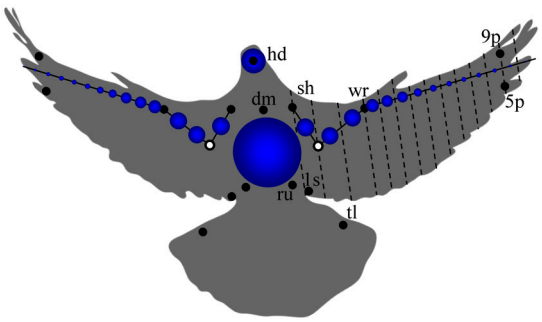

Fig. 3. Pigeon marker locations and mass-distribution model. Silhouette at middownstroke with 16 marker locations (solid black circles) and calculated elbow locations (open circles). The approximate wingstrip edges (dashed lines) and marker descriptors are provided for the bird's right side (dm: dorsal midshaft; ru: rump; sh: shoulder, 5 p: fifth primary; 9 p: ninth primary; tl: tail; 1 s: innermost secondary; see *Methods* for details). Modeled point masses (blue spheres), with size representing relative mass. Note that the tail is considered part of the torso mass (largest blue sphere).

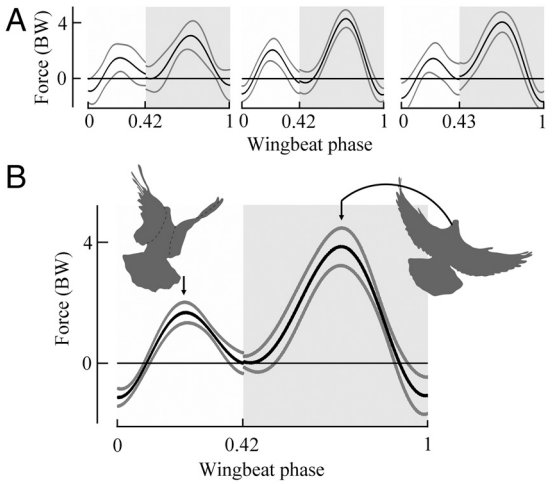

Fig. 4. Net aerodynamic force magnitude (|**F**|) in line with the stroke-averaged aerodynamic force for turning pigeons. The force magnitude is normalized to body weight (BW) and wingbeat duration. Gray shading indicates downstroke. (*A*) Mean |**F**| ± SD (n = 20) for each of three individual pigeons. (*B*) Pooled mean ± SD of the mean |**F**| across the three pigeons. Representative silhouette at both phases of upstroke and downstroke peak force (black arrows) illustrates timing with respect to wing configuration. Note that the discontinuity between upstroke and downstroke traces results from normalization to the half-stroke phases, necessitated by variations in stroke durations.

aerodynamic forces were directed vertically to support the pigeon's body weight and horizontally to change its flight trajectory during the turn (Fig. 2).

Substantial Body Rotations Occur About All Three Anatomical Axes. The 3D body rotations of the turning pigeons consisted of substantial roll, pitch, and yaw components, defined as rotations about the antero-posterior (along the spine), the medio-lateral, and dorso-ventral body frame axes, respectively (19) (Table 1 and Fig. 1). During the turn, body rotations oscillated back and forth within wingbeats but led to net changes in body orientation between successive wingbeats. The pigeons' 3D body rotations predominantly consisted of roll, both continuously and on a net wingbeat basis, although pitch and yaw components were also substantial (Table 1). Over the course of a turn, early wingbeats

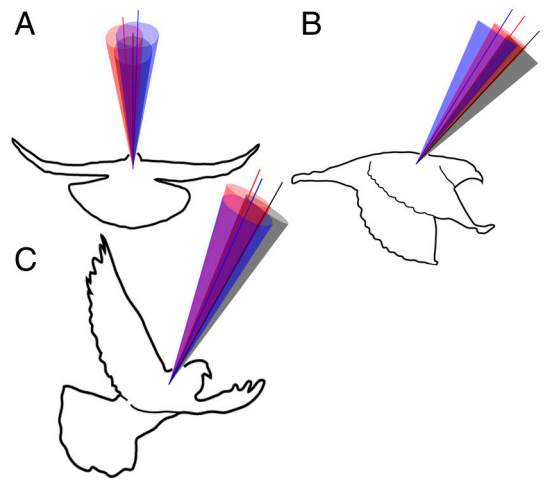

Fig. 5. Mean net downstroke aerodynamic forces ($\mathbf{F}_d$) for three turning pigeons expressed in the body frame and superimposed on a pigeon outline. The mean ± SD vector cone is depicted by a different color for each individual averaged for all analyzed wingbeats of the turns. For clarity, three views are provided: (*A*) rear view, (*B*) side view, and (*C*) oblique view.

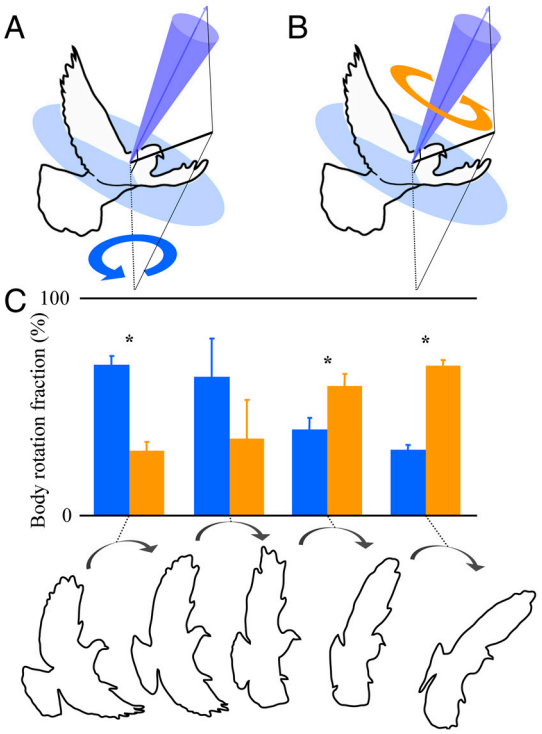

Fig. 6. Decomposition of sequential body rotations of a turning pigeon. (*A* and *B*) Outline of a pigeon, with superimposed $\mathbf{F}_d$ and SD vector cone, as well as the plane to which $\mathbf{F}_d$ is normal, and an exemplary axis of body rotation (thick black line), all in the body frame. (*A*) The component of the body rotation that redirects $\mathbf{F}_d$ (blue circular arrow). Note that the axis describing this rotation fraction lies within the circular blue plane. (*B*) The component of the body rotation about $\mathbf{F}_d$ (orange circular arrow). (*C*) Fractions of body rotation for four sequential, complete wingbeats of the turn, showing the orthogonal components of body rotations that redirect $\mathbf{F}_d$ (blue fraction) versus which occur about $\mathbf{F}_d$ (orange fraction). Pooled mean ± SD of means of three individuals. Middownstroke outlines of five sequential wingbeats, as seen from a single elevated viewpoint from inside the turn. Gray arrows and dotted lines link colored bars to positions in the turn. Asterisks indicate significant differences between body rotation fractions.

rolled the pigeons into the turn, with subsequent wingbeats producing net roll rotations out of the turn. In contrast, net wingbeat rotations about the pitch and yaw axes were directed upward and into the turn, respectively, throughout turning. Oscillations of body rotations within wingbeats were larger in pitch and roll (16 ± 5 and 13 ± 6°/wingbeat, respectively) and smallest in yaw (4 + 3°/wingbeat), indicating yaw angular velocities were most uniform.

Pigeons Produce Consistent Patterns of Aerodynamic Force. The directions and magnitudes of instantaneous net aerodynamic force (**F**) exhibited stereotypic patterns within the body frame during both downstroke and upstroke (Figs. 2*D*, 4, and 5). During downstroke **F** was directed mainly in the midsagittal plane of the birds, whereas during upstroke **F** was more variably directed. Net aerodynamic force magnitude (|**F**|) approximated zero at the upstroke-downstroke transition before peaking near middown-

Table 1. Body rotations accumulated throughout the turn

Body rotations	Continuous effects (deg)	Net wingbeat effects (deg)
Roll	143 ± 16	77 ± 14
Pitch	125 ± 24	43 ± 2
Yaw	81 ± 10	58 ± 4

Mean ± SD of means of three individuals for both continuous and net wingbeat effects in terms of roll, pitch, and yaw.

stroke [4.5 ± 0.4 body weights (BW) at 53% of the downstroke period] (Fig. 4). At the downstroke-upstroke transition, $\mathbf{F}$ momentarily opposed the stroke average. Throughout the remainder of the upstroke, however, the pigeons produced aerodynamic force in support of body weight, in line with the stroke average. $|\mathbf{F}|$ reached a maximum at midupstroke ($2.3 + 0.3$ BW, Fig. 4), coinciding with tip reversal (Fig. 4*B*, left silhouette). Although upstroke peak $|\mathbf{F}|$ averaged about half the downstroke peak $|\mathbf{F}|$, the aerodynamic impulse generated during upstroke averaged $27 \pm 4\%$ of the impulse generated during downstroke. Aerodynamic forces averaged 1.33 ± 0.07 BW over the full wingbeat cycle, consistent with the pigeons' need for centripetal forces in addition to weight support to fly through the turn. A sensitivity analysis consisting of a decrease and an increase of the wing masses by 10% resulted in an increase and a decrease of upstroke peak force estimate by approximately 5%, respectively, indicating the robustness of our findings for upstroke aerodynamic force based on the full body and wing mass-distribution model of the birds.

As the pigeon rotated its body and changed its flight trajectory, downstroke-averaged aerodynamic forces ($\mathbf{F}_d$) were produced in a uniform direction with respect to the pigeon's body during the five sequential wingbeats of the turn (Fig. 5). $\mathbf{F}_d$ were oriented in the midsagittal plane of the bird's body and directed anterior to the dorso-ventral body axis by $38 + 7°$ (Fig. 5), consistent with the "pitched-up" body orientation of pigeons during slow steady flight (approximately 32° at a flight speed of 5–6 ms^{-1}) (20). During slow flight aerodynamic drag is small and, by approximation, only gravity needs to be countered by near vertical aerodynamic forces.

Turning Pigeons Prioritize Changes in Trajectory over Angular Positioning of the Body. By comparing rotations of the pigeon's torso with respect to redirection of $\mathbf{F}_d$ over the course of a wingbeat in the global frame, we evaluated the extent to which pigeons relied on body rotations to redirect $\mathbf{F}_d$ versus to what extent body rotations occurred about the direction of $\mathbf{F}_d$ (see *Methods* for details). Body rotations that redirect $\mathbf{F}_d$ alter flight trajectory, but body rotations about $\mathbf{F}_d$ leave the direction of $\mathbf{F}_d$ in the global frame unaffected and therefore do not change flight trajectory. This analysis revealed that for each sequential wingbeat of the turn, the pigeon's body progressively rotated about an axis that was increasingly aligned with the direction of $\mathbf{F}_d$ (Fig. 6). Body rotations produced over the course of the first two wingbeats of the turn predominantly redirected $\mathbf{F}_d$ ($70.1 \pm 4.1\%$ and $64.4 \pm 17.8\%$, respectively), whereas body rotations during the last two wingbeats occurred predominantly about $\mathbf{F}_d$ ($60.2 \pm 5.6\%$ and $69.4 \pm 2.3\%$) (Fig. 6*C*).

In summary, during turning flights the pigeon's torso oscillated vigorously due to the combined effect of the flapping wings (resulting from inertial forces) and aerodynamic forces in relation to gravity. Aerodynamic forces accelerating the bird's center of mass peaked during downstroke but also peaked during upstroke and were roughly half the downstroke magnitude. These aerodynamic forces serve to offset gravity and change the bird's flight trajectory to achieve level 90° turns. Even though the pigeon's orientation changed significantly about all three body axes, downstroke-averaged aerodynamic forces were produced in a uniform anatomical direction. Decomposition of successive wingbeat 3D body rotations revealed that early in the turn body rotations of the pigeon mainly redirected downstroke-averaged aerodynamic forces, reflecting anatomical constraints on the direction of aerodynamic force production. However, later in the turn body rotations mainly served to reorient the bird's body for straight flight and had little effect on the direction of aerodynamic force production.

Discussion

Using an analytical approach based on high-speed 3D kinematics and detailed body mass distributions, we determined the time-varying net aerodynamic forces produced by slowly flying pigeons as they negotiated 90° level turns (Fig. 2). We identified the tip-reversal upstroke as aerodynamically active (Figs. 2 and 4*B*), indicating its role for increased power production and control of body position. Net aerodynamic forces were produced in a uniform direction within the pigeon's body frame, requiring that changes in flight trajectory be mediated by body rotations that redirect aerodynamic force in the global frame (Fig. 5). Consistent with our hypothesis, the overall turning strategy consisted of force vectoring to change the pigeon's flight trajectory, followed by reacquisition of the bird's preferred body orientation for forward flight (Fig. 6).

Substantial rotations occurred about all three anatomical axes indicating that (*i*) pigeons are not restricted to a particular anatomical axis to change their body orientation, and (*ii*) body rotations function to redirect net aerodynamic forces as needed to negotiate the turn (Table 1). That body rotations occurred mainly about the birds' roll axis does not necessarily reflect a preference for this axis but may simply reflect the birds' body orientation upon entering the turn and the reliance on force vectoring to negotiate the turn.

Net Aerodynamic force magnitude ($|\mathbf{F}|$) varied consistently, with minima and maxima occurring at wingbeat phases as predicted by aerodynamic theory (21) across all individuals and trials. The average net aerodynamic force per wingbeat was greater than one BW because turning birds need to accelerate themselves to redirect their flight trajectory as well as offset their weight due to gravity. The small negative peak in $|\mathbf{F}|$, opposing the stroke-averaged aerodynamic force, may well reflect an aerodynamic consequence of strong supination of the wings near the downstroke-upstroke transition (22).

Positive aerodynamic force during the upstroke coincided with wing tip reversal (Fig. 4*B*, left silhouette). During an upstroke with tip reversal, the elbow and wrist are flexed, and the hand-wing is supinated, causing it to be inverted. Elbow and wrist flexion effectively moves the point of wing rotation from the shoulder during the downstroke toward the wrist during the upstroke, facilitating the upward "back flick" of the hand-wing. This tip reversal mechanism is found in the slow to intermediate flight of birds with relatively pointed wings as well as some birds with rounded wings (22–24) and bats (10, 25, 26). The functional significance of wing tip reversal has been the subject of debate since the pioneering work of Brown (27) and has been proposed by others in prior studies of avian flight to be aerodynamically active (10, 24–34). Until now, however, aerodynamic force production of the tip reversal upstroke had not been convincingly demonstrated during vertebrate flight.

The consistent force patterns observed here across wingbeats of all three pigeons provide definitive evidence for upstroke aerodynamic force production during slow flight in birds larger than hummingbirds (Fig. 2, 4). Useful contributions of an active tip-reversal upstroke to weight support can therefore be expected during other modes of flight where tip reversal is present, such as hovering, landing, and steady slow flight. This is reinforced by the fact that we observed no significant differences in upstroke force patterns across the five wingbeats during which birds entered, executed, and left the 90° turn. Aerodynamic force generation by the tip-reversal mechanism also agrees with recent force measurements of pigeon wings spun like a propeller while positioned in an upstroke configuration (35).

Although maximum $\mathbf{F}$ during the upstroke reached 50% of maximum $\mathbf{F}$ during the downstroke (Fig. 4), the upstroke generated only $27 \pm 4\%$ of the downstroke impulse. The smaller impulse of the upstroke reflects its shorter period (42% of the wingbeat duration) as well as the opposing aerodynamic force

production relative to weight support early in the upstroke (Fig. 4*B*).

In a comparative context, the relative contribution of upstroke aerodynamic force to total impulse in pigeons is nevertheless surprisingly high. Hummingbirds operate at temporal and spatial scales similar to insects (2) and, until recently, were thought to share weight support between the two halves of the wingbeat (36). However, hovering rufous hummingbirds generate only 33% of the downstroke impulse during upstroke [(37), based on wake measurements]. With an upstroke that generates 27% of their downstroke impulse, pigeons achieve a similar impulse distribution to that found in rufous hummingbirds, which is remarkable because hummingbirds are thought to have evolved a highly derived upstroke (38).

Our hypothesis that pigeons produce aerodynamic forces in a uniform anatomical direction is also clearly supported (Fig. 5). $\mathbf{F}_d$ was oriented within the midsagittal body plane and directed antero-dorsally, with little variation across successive turning wingbeats. Thus, during low speed flight, pigeons exhibit a consistent direction of net aerodynamic force production with respect to their bodies, reflecting the fundamental anatomical features that underlie powered avian flapping flight.

The constrained direction of force production in the body frame indicates that pigeons turn much like insects and helicopters. Helicopters redirect aerodynamic forces relative to their fuselage (in the body frame) within relatively narrow ranges (roughly 20°) (39), meaning that maneuvers with more substantial redirections of resultant forces in the global frame require force vectoring, as we found for pigeons. Airplanes, with decoupled wing lift and engine thrust, can redirect resultant forces to a larger degree within the body frame, particularly in the fore-aft direction (for modern fighter planes this can be >90°) (40), reducing their reliance on force vectoring to maneuver.

The turning strategy of pigeons appears to prioritize trajectory changes over readjustments of body orientation. Body rotations of the pigeons early in the turn mainly contribute to changes in flight trajectory, whereas body rotations progressively later in the turn predominantly serve to realign the body for subsequent forward flight, having a smaller effect on redirecting aerodynamic force (Fig. 6*C*). This turning strategy likely arises from constraint of $\mathbf{F}_d$ direction with respect to the bird's body, which requires force vectoring to redirect $\mathbf{F}_d$. However, body rotations that redirect $\mathbf{F}_d$ during the first part of the turn result in a body orientation that is not well suited for the bird's new flight trajectory. Therefore, once the bird achieves its new target flight trajectory, its preferred body orientation for forward flight must be reacquired by rotating its body about $\mathbf{F}_d$. Only body rotations that occur about $\mathbf{F}_d$ leave the newly acquired flight trajectory unaffected, which explains why these body rotations predominantly occur later in the turn.

To the extent that aerodynamic force production may be anatomically constrained in avian flapping flight, it seems likely that the pattern of early flight trajectory adjustment followed by reacquisition of a preferred forward flight body orientation observed here for slow turning flight may also apply for fast turning flight. At higher flight speeds, however, changes in wings and/or tail configurations are likely to produce more substantial changes in aerodynamic force with respect to the bird's body (41), allowing for changes in aerodynamic force direction, independent of force vectoring, to achieve a turn. Additionally, given that flight power requirements are lowest at intermediate speeds (42), birds may be able to redirect aerodynamic force within the body frame by differentially activating flight muscles between their inside and outside wings. This could enable an alternative turning strategy to that observed here. For instance, during flight versus when flap-running, chukars produced aerodynamic forces roughly in the same global direction, yet body pitch orientation differs by about 30° between these behaviors (43). These findings indicate that birds may be able to redirect aerodynamic forces more variably with respect to the body depending on behavior or power output.

At the low flight speeds examined here, pigeons operate much like helicopters, which have limited capacity to redirect aerodynamic forces relative to their bodies, relying on whole-body force vectoring to change flight trajectory, similar to fruit flies, blow flies, and house flies (5, 7, 44, 45). The moderate redirection of $\mathbf{F}_d$ with respect to the pigeon's body that does occur may contribute to body torques required to produce the body rotations needed for turning (11,12). Understanding flight control will therefore require insight into the specific mechanisms used by pigeons to generate the torques that produce the observed body rotations. However, torques cannot be inferred from Newton's second law of motion because the distribution of applied forces remains unknown. Nevertheless, by limiting the direction of aerodynamic force production to a single main axis relative to the body, our results indicate that birds may simplify the problem of controlling turns from six to four degrees of freedom (46).

Methods

Three rock doves (*Columba livia*) were selected from 10 wild-caught individuals, based on subjective assessment of their initial turning flight performance during training. These pigeons were housed, trained, and studied at the Concord Field Station (Bedford, MA) in accordance with protocols approved by Harvard University's Institutional Animal Care and Use Committee. The pigeons were trained to fly back and forth between two perches situated at either end of two 5-m-long by 1-m-wide by 2-m-high netted sections, connected by a 90° turn midway (Fig. 2*B*). The symmetrical, square-corner corridor was constructed of lightweight, 2-cm mesh nylon deer netting supported by a PVC frame consisting of 4-cm diameter piping.

Using nine synchronized high-speed cameras, 3D positions of body markers were collected within a calibrated 1.8 m^3 cubic volume that encompassed the turn. Trials accepted for analysis were those in which the birds (*i*) did not contact the netting and (*ii*) maintained a turning flight trajectory relative to global horizontal of <5°. The pigeons were marked at 16 anatomical locations (Fig. 3): dorsum at the second thoracic vertebra (dm); left and right rump (4-cm lateral to the vertebral column over the synsacrum) (ru); center of head (hd); left and right wing roots (sh); left and right wrists (wr); tip of left and right fifth primary feathers (5 p); 67% of the length of left and right ninth primary feathers (9 p); 67% along the length of left and right outer tail feathers (tl); left and right tip of the innermost secondary feathers (1s). Elbow position was determined trigonometrically based on two lengths and three positions: brachial and antebrachial segment lengths and wing root, wrist, and tip of the innermost secondary feather positions. Flights were recorded with two camera systems: a high-speed light video system recording at 250 Hz with 0.001 sec exposure time, consisting of one FastCam-X 1280 PCI and two FastCam 1024 PCI cameras (Photron USA Inc.), and an infrared-based auto-tracking system recording at 240 Hz with 0.0004 sec exposure time, consisting of six ProReflex MCU240 cameras (Qualisys AB). The two camera systems were synchronized using a start trigger signal. The visible-light videos were digitized using DLTdv3 (47). Calculations were performed in Matlab (Mathworks Inc.) using custom-written scripts. Positional data were filtered with a fourth-order Butterworth filter using a low-pass cutoff frequency three times the wingbeat frequency. Cutoff frequency was determined by residual analysis (48).

Rotations. The sum of absolute back and forth rotations within a wingbeat and the net change in body orientation over a wingbeat period were defined as continuous and net wingbeat body rotations, respectively, about each of the body axes. For each turn, five sequential wingbeats were analyzed, during which continuous and net wingbeat body rotations about each axis were accumulated.

Aerodynamic Forces. The position of the net CM was approximated throughout the turn using a mass-distribution model of the body and tail, head, and wings (Fig. 3). The torso and tail were represented by a single point-mass, because the effect of tail movements on net CM were assumed to be minor and are difficult to model. The head and 14 chordwise strips per wing were modeled as point-masses, with time-varying positions based on segment kinematics (Fig. 3). The two wings together constitute approximately 1/8th of a pigeon's body mass. The motion of the flapping wings causes the net CM to move substantially relative to a pigeon's torso CM, necessitating the time-dependent, non-body-fixed CM calculations.

Wingbeats were partitioned into upstroke and downstroke phases, based on reversal of the major bending direction of the primary feathers. This bending reversal of the primary feathers coincided with the instant the primary feather markers moved laterally relative to the body, in both ventral (start of upstroke) and dorsal (start of downstroke) positions.

Instantaneous net aerodynamic forces (**F**) were determined throughout the turn based on net CM accelerations relative to gravity, because the CM of a freely flying bird can only be accelerated by external gravitational and aerodynamic forces. **F** vectors were normalized to wingbeat phase and expressed in the body frame. The net aerodynamic forces averaged over the duration of the downstroke ($\mathbf{F}_d$) act in line with the main impulse vector, the time integral of force, produced during each wingbeat.

Redirection of Aerodynamic Forces Versus Rotation About Aerodynamic Forces. Identification of $\mathbf{F}_d$ allowed for decomposition of body rotations relative to this direction of main aerodynamic impulse imparted during each downstroke. Body rotations of the bird were analyzed with respect to $\mathbf{F}_d$ over the five wingbeats of the turn. Two 3D rotations were calculated between successive middownstroke instants of each wingbeat: a 3D body rotation and a 3D redirection of $\mathbf{F}_d$. Body rotations identical to the redirection of $\mathbf{F}_d$ were designated as representing 100% redirection of $\mathbf{F}_d$. Conversely, if body rotations did not redirect $\mathbf{F}_d$, body rotations were designated as representing 100% rotation about $\mathbf{F}_d$. Mathematically, this approach is identical to expressing the 3D body rotation as a vector in the body frame and determining the relative magnitudes of two perpendicular projections of this vector: (*i*) The projection of the 3D body rotation vector on the plane normal to $\mathbf{F}_d$ represents the component of the body rotation that redirects $\mathbf{F}_d$ (force vectoring), and (ii) the projection of the 3D body rotation vector on $\mathbf{F}_d$ represents the component of the body rotation about $\mathbf{F}_d$. This approach allowed any 3D body rotation to be decomposed into two complementary body rotation fractions, one that redirected $\mathbf{F}_d$ and one that rotated about $\mathbf{F}_d$ (Fig. 6 *A* and *B*).

Statistics. All results were are based on five complete wingbeats nearest the center of each of two left and two right turns for each individual (20 wingbeats per bird, $N = 3$) expressed as mean $\pm$ SD. Paired t-tests (JMP, SAS Institute) were used to compare group means for the three individuals. Differences were considered significant when $p < 0.05$.

ACKNOWLEDGMENTS. We thank P. A. Ramirez for care of the animals, D. E. Lieberman for shared use of the Qualysis cameras, and A. N. Ahn, D. R. Warrick, A. S. Arnold-Rife, C. A. Moreno, T. E. Higgins, A. Eberle, C. Gastil, A. Randall, and the Rotary Wing Forum for helpful discussions and informal contributions to this work. We furthermore thank three anonymous reviewers for their constructive suggestions. This research was funded by National Science Foundation Grant IOS-0744056 to A.A.B.

1. Arbib MA, Érdi P, Szentágothai J (1997) *Neural Organization: Structure, Function, and Dynamics* (Bradford Book/MIT, Cambridge, MA).
2. Dudley R (2000) *The Biomechanics of Insect Flight. Form, Function, Evolution* (Princeton Univ Press, Princeton, NJ).
3. Mayer M, Vogtmann K, Bausenwein B, Wolf R, Heisenberg M (1988) Flight control during 'free yaw turn' in *Drosophila melanogaster*. *J Comp Physiol A* 163:389–399.
4. Blondeau J (1981) Aerodynamic capabilities of flies, as revealed by a new technique. *J Exp Biol* 92:155–163.
5. Götz KG, Wandel U (1984) Optomotor control of force and light in *Drosophila* and *Musca*, II Covariance of lift and thrust in still air. *Biol Cybern* 51:135–139.
6. Sugiura H, Dickinson MH (2009) The generation of forces and moments during visually-evoked steering maneuvers in flying *Drosophila*. *PLoS ONE* 4:e4883.
7. Wagner H (1986) Flight performance and visual control of flight of the freeflying housefly (*Musca domestica* L.). I. Organization of the flight motor. *Philos Trans R Soc Lond B Biol Sci* 312:527–551.
8. Collett TS, Land MF (1975) Visual control of flight behaviour in the hoverfly, *Syritta pipiens* L. *J Comp Physiol A* 99:1–66.
9. Nachtigall W (1979) Schiebeflug bei der Schmeißfliege *Calliphora erythrocephala* (Diptera: Calliphoridae). *Entomol Gen* 5:255–265.
10. Aldridge HDJN (1986) Kinematics and aerodynamics of the Greater Horseshoe Bat (*Rhinolopus ferrumequinum*) in horizontal flight at various flight speeds. *J Exp Biol* 126:479–497.
11. Warrick DR, Dial KP (1998) Kinematic, aerodynamic and anatomical mechanisms in the slow, maneuvering flight of pigeons. *J Exp Biol* 201:655–672.
12. Hedrick TL, Biewener AA (2007) Low speed maneuvering flight of the rose-breasted cockatoo (*Eolophus roseicapillus*). I. Kinematic and neuromuscular control of turning. *J Exp Biol* 210:1897–1911.
13. Iriarte-Diaz J, Swartz SM (2008) Kinematics of slow turn maneuvering in the fruit bat *Cynopterus brachyotis*. *J Exp Biol* 211:3478–3489.
14. Berg AM, Biewener AA (2010) Wing and body kinematics of takeoff and landing flight in the pigeon (*Columba livia*). *J Exp Biol* 213:1651–1658.
15. Sy M (1936) Funktionell-anatomische Untersuchungen am Vogelflügel. *Journal für Ornithologie* 84:199–296.
16. Rayner JMV (1988) The evolution of vertebrate flight. *Biol J Linn Soc* 34:269–287.
17. Dial KP, Goslow GE, Jenkins FA (1991) The functional anatomy of the shoulder in the European starling (*Sturnus vulgaris*). *J Morphol* 207:327–344.
18. Gatesy SM, Baier DB (2005) The origin of the avian flight stroke: A kinematic and kinetic perspective. *Paleobiology* 31:382–399.
19. Phillips WF (2004) *Mechanics of Flight* (Wiley, Hoboken, NJ).
20. Biewener AA, Corning WR, Tobalske BW (1998) *In vivo* pectoralis muscle force-length behavior during level flight in pigeons (*Columba livia*). *J Exp Biol* 201:3293–3307.
21. Greenewalt CH (1975) The flight of birds: The significant dimensions, their departure from the requirements for dimensional similarity, and the effect on flight aerodynamics of that departure. *T Am Philos Soc* 65:1–67.
22. Brown RHJ (1963) The flight of birds. *Biol Rev* 38:460–489.
23. Zimmer K (1943) Der Flug des Nektarvogels (*Cinnyris*). *Journ F Orn* 91:371–387.
24. Tobalske BW (2007) Biomechanics of bird flight. *J Exp Biol* 210:3135–3146.
25. Norberg UM (1976) Aerodynamics, kinematics, and energetics of horizontal flapping flight in the long-eared bat *Plecotus auritus*. *J Exp Biol* 65:179–212.
26. Norberg UM (1990) *Vertebrate Flight* (Springer, Berlin).
27. Brown RHJ (1948) The flapping cycle of the pigeon. *J Exp Biol* 25:322–333.
28. Alexander RM (1986) *Animal Mechanics* (Univ Washington Press, Seattle).
29. Azuma A (1992) *The Biokinetics of Flying and Swimming* (Springer, New York).
30. Bundle MW, Dial KP (2003) Mechanics of wing-assisted incline running (WAIR). *J Exp Biol* 206:4553–4564.
31. Hedrick TL, Usherwood JR, Biewener AA (2004) Wing inertia and whole-body acceleration: an analysis of instantaneous aerodynamic force production in cockatiels (*Nymphicus hollandicus*) flying across a range of speeds. *J Exp Biol* 207:1689–1702.
32. Iriarte-Diaz J, Riskin DK, Willis DJ, Breuer KS, Swartz SM (2011) Whole-body kinematics of a fruit bat reveal the influence of wing inertia on body accelerations. *J Exp Biol* 214:1546–1553.
33. Lorenz KZ (1933) Beobachtetes über das Fliegen der Vögel und über die Beziehungen der Flügel- und Steuerform zur Art des Fluges. *Journal für Ornithologie* 81:107–236.
34. Spedding GR, Rayner JMV, Pennycuick CJ (1984) Momentum and energy in the wake of a pigeon (*Columba livia*) in slow flight. *J Exp Biol* 111:81–102.
35. Crandell KE, Tobalske BW (2011) Aerodynamics of tip-reversal upstroke in a revolving pigeon wing. *J Exp Biol* 214:1867–1873.
36. Weis-Fogh T (1972) Energetics of hovering flight in hummingbirds and in *Drosophila*. *J Exp Biol* 56:79–104.
37. Warrick DR, Tobalske BW, Powers DR (2005) Aerodynamics of the hovering hummingbird. *Nature* 435:1094–1097.
38. Stolpe M, Zimmer K (1939) Der Schwirrflug des Kolibri im Zeitlupenfilm. *J Orn* 87:136–155.
39. Talbot PD, Corliss LD (1977) *A Mathematical Force and Moment Model of a UH-1H Helicopter for Flight Dynamics Simulations* NASA Technical Memo-73, 254.
40. Winchester J (2006) *The Encyclopedia of Modern Aircraft: From Civilian Airliners to Military Superfighters* (Thunder Bay Press, San Diego).
41. Rüppell G (1977) *Bird Flight* (Von Nostrand Reinhold, New York).
42. Tobalske BW, Hedrick TL, Dial KP, Biewener AA (2003) Comparative power curves in bird flight. *Nature* 421:363–366.
43. Dial KP, Jackson BE, Segre P (2008) A fundamental avian wing-stroke provides a new perspective on the evolution of flight. *Nature* 451:985–990.
44. Fry SN, Sayaman R, Dickinson MH (2003) The aerodynamics of free-flight maneuvers in *Drosophila*. *Science* 300:495–498.
45. Vogel S (1966) Flight in *Drosophila*. I. Flight performance of tethered flies. *J Exp Biol* 44:567–578.
46. LaValle SM (2006) *Planning Algorithms* (Cambridge, Cambridge, UK).
47. Hedrick TL (2008) Software techniques for two- and three-dimensional kinematic measurements of biological and biomimetic systems. *Bioinspir Biomim* 3:034001.
48. Winter DA (2005) *Biomechanics and Motor Control of Human Movement* (Wiley, Hoboken).